Synthesis and biological evaluation of 4-hydroxy-methylpiperidinyl-N-benzyl-acylarylhydrazone hybrids designed as novel multifunctional drug candidates for Alzheimer's disease

Synthesis and biological evaluation of 4-hydroxy-methylpiperidinyl-*N*-benzyl-acylarylhydrazone hybrids designed as novel multifunctional drug candidates for Alzheimer's Disease

Sarah Macedo Vaz[a], Matheus de Freitas Silva[a], Marcos Jorge R. Guimarães[b], Fernanda Motta R. da Silva[b], Newton Gonçalves Castro[b], Isabella Alvim Guedes[c], Laurent E. Dardenne[c], Marina Amaral Alves[d], Rafael Garrett da Costa[d], Gabriela Beserra Pinheiro[e], Letícia Germino Veras[e], Márcia Renata Mortari[e], Letizia Pruccoli[f], Andrea Tarozzi[f] and Cláudio Viegas Jr. [a*]

[a] PeQuiM - Laboratory of Research in Medicinal Chemistry, Institute of Chemistry, Federal University of Alfenas, MG 37133-840, Brazil

[b] Laboratory of Molecular Pharmacology, Institute of Biomedical Sciences, Federal University of Rio de Janeiro, RJ 21941-902, Brazil

[c] National Laboratory for Scientific Computing - LNCC, Petropolis, RJ 25651-075, Brazil.

[d] Laboratory of Metabolomics – LabMeta/LADETEC, Institute of Chemistry, Federal University of Rio de Janeiro, RJ 21941-598, Brazil

[e]Laboratory of Neuropharmacology, Institute of Biological Sciences, University of Brasília, Brasilia, DF 70910-900, Brazil

[f]Department for Life Quality Studies, Alma Mater Studiorum – University of Bologna, Rimini, 47921, Italy.

ABSTRACT

The search for new drug candidates against Alzheimer's disease (AD) remains a complex challenge for medicinal chemists due to its multifactorial pathogenesis and incompletely understood physiopathology. In this context, we have explored the molecular hybridization of pharmacophore structural fragments from known bioactive molecules, aiming to obtain a novel molecular architecture in new chemical entities capable of concomitantly interacting with multiple targets in a so-called multi-target directed ligands (MTDLs) approach. This work describes the synthesis of 4-hydroxymethyl)piperidine-*N*-benzyl-acyl-hydrazone derivatives **5a-l**, designed as novel MTDLs, showing improved multifunctional properties compared to the previously reported parent series of *N*-benzyl-(3-hydroxy)piperidine-acyl-hydrazone derivatives **4**. The new improved derivatives were studied *in silico*, regarding their mode of interaction with AChE enzyme, and *in vitro*, for evaluation of their effects on the selective inhibition of cholinesterases, cellular antioxidant and neuroprotective activities as their cytotoxicity in human neuroblastoma (SH-SY5Y) cells. Overall, compound PQM-181 (**5k**) showed the best balanced selective and non-competitive inhibition of AChE (IC_{50}= 5.9 μM, SI > 5.1), with an additional antioxidant activity (IC_{50}= 7.45 μM) against neuronal *t*-BOOH-induced oxidative stress and neuroprotective ability against neurotoxicity elicited by both *t*-BOOH and OAβ_{1-42}, and a moderate ability to interfere in Aβ_{1-42} aggregates, with low cytotoxicity and good predictive druggability properties, suggesting a multifunctional pharmacological profile suitable for further drug development against AD.

Keywords: multifunctional drug, MTDLs, AChE inhibitors, neuroprotection, Alzheimer's disease.

1. Introduction

Alzheimer's disease (AD) is the most common neurodegenerative condition in the elderly, characterized by massive atrophy and loss of brain mass and neurons with a progressive impairment of cognitive functions and memory, behavioural instability, leading to generalized incapacity and death[1]. The onset and progression of AD are related to multiple and interconnected physiological and biochemical factors, such as decrease in acetylcholine (ACh) production, combined by extracellular deposition of β-amyloid (Aβ) peptide aggregates, intracellular neurofibrillary tangles constituted by over phosphorylated tau protein, oxidative stress (OS) and neuroinflammation [1–3]. Recent studies have suggested that soluble Aβ aggregates (protofibrils and oligomers) diffuse in the brain parenchyma and alter synaptic function, with selective neuronal losses in the cortex and hippocampus, which are most characteristically affected regions in AD [4–10]. Among the mechanisms of toxicity mediated by Aβ peptide, the accumulation of reactive oxygen species (ROS) and impairment of the cellular redox status play an important role in triggering neuronal death. In this regard, several studies show that ROS formation is derived from direct interactions between Aβ and metals and indirect interactions with the electron transport chain of mitochondria, leading to lower activity of secretase enzymes, inducing the production of Aβ and creating a complex cycle of interconnected events that reinforce OS, and neuronal death. [11–14]. Nowadays, there is a consensus that AD and other neurodegenerative diseases (NDs) are clearly multifactorial, involving a pathogenesis-based complex interconnected physiological, biochemical and chemical changes, mediated by different activation pathways [15], which could, in turn, explain the inefficiency of current therapeutics. The polypharmacology concept, in which multiple pathological events are treated with the use of two or more drugs or two or more active ingredients in the same formulation, has significant limitations, particularly in the elderly. Thus, a new paradigm has emerged for treating multifactorial pathology, focusing on the rational design of single drug-containing structural attributes that guarantee the concomitant modulation of multiple molecular targets [16–23].

We recently reported the discovery of an innovative series of hybrid 3-hydroxy-piperidine-*N*-arylacylhydrazone derivatives (**4**, Figure 1), designed by molecular hybridization (MH) of the functionalized piperidine pharmacophore subunit present in the structure of the anti-Alzheimer drug donepezil (**1**) and the acetylcholinesterase (AChE) inhibitor LASSBio-767 (**2**) and the *N*-acyl-arylhydrazone subunit as a privileged structure present in several anti-inflammatory ligands (**3**). Some of these new compounds exhibited an interesting multifunctional activity, acting as AChE inhibitors with additional neuroprotective and anti-inflammatory properties [24]. Based on their unique structural framework and promising biological properties, we designed another series of optimized analogues (**5**, Figure 1), aiming to eliminate the stereogenic centre at the C-3 position of the 3-hydroxy-piperidine ring (e) by changing it for an aquiral 4-hydroxymethyl-piperidine system (f). In addition, based on previous molecular docking studies (data not shown), which indicated that an extended hydroxylated side chain in the piperidine system could lead to higher ligand-enzyme affinity in comparison to the original

series **4** due to additional beneficial interactions between the hydroxy group and amino acid residues on the active site of AChE, we decided to explore the possible improved pharmacological profile resultant from the introduction of a methylene-hydroxy substituent at the C-4 position of the *N*-benzylpiperidine pharmacophore (f, Figure 1). Besides, we also varied the position of substituents (R) in the aromatic ring of the arylhydrazone subunit (g), aiming to evaluate the contribution of regiochemistry in the biological activity, in comparison to the most active *para*-substituted compounds PQM-56 (**4c**), PQM-57 (**4d**), PQM-67 (**4g**) and PQM-75 (**4j**) from the original series **4** [24] (Figure 1). Thus, we expected that this simplified molecular scaffold could lead to the discovery of novel optimized multifunctional drug candidate prototypes with easy synthetic access and low toxicity.

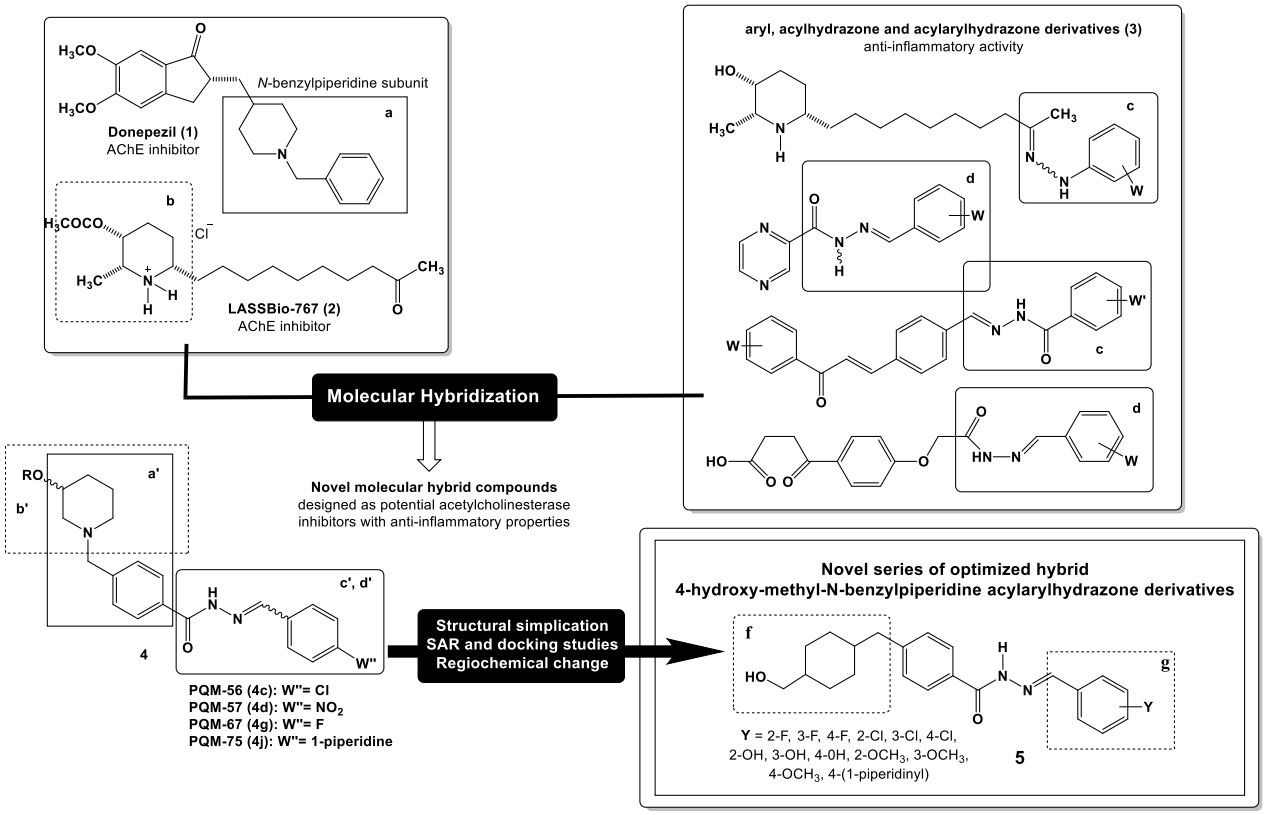

Figure 1. Design of a new series **4** of MTDLs based on the molecular hybridization of the structures of donepezil (**1**), the AChE inhibitor LASSBio-767 (**2**) and a series of anti-inflammatory *N*-aryl-acylhydrazone derivatives (**3**) and structural optimization to generate the related series of novel 4-hydroxy-methylpiperidinyl-*N*-benzyl-acylarylhydrazones (**5**).

2. Results and discussion

2.1. Chemistry

The synthetic route for the target compounds is outlined in Scheme 1. In a first step, commercial methyl 4-formylbenzoate (**6**) was submitted to a reductive amination reaction with 4-piperidine-methanol (**7**), in the presence of $NaBH_3CN$ and $ZnCl_2$ in dry MeOH, leading to the correspondent *N*-benzylpiperidine ester **8** in a 66% yield after purification by flash column chromatography (CC). The ester **8** was then reacted with hydrazine monohydrate, furnishing

the hydrazide **9** as a key-intermediate in 93% yield after purification by CC. In a final divergent step, key hydrazide **9** was coupled to different functionalized benzaldehydes (**10a-l**) substituted in the 2-, 3- and 4-positions to generate the desired target compounds **5a-l** in 21-86% yields.

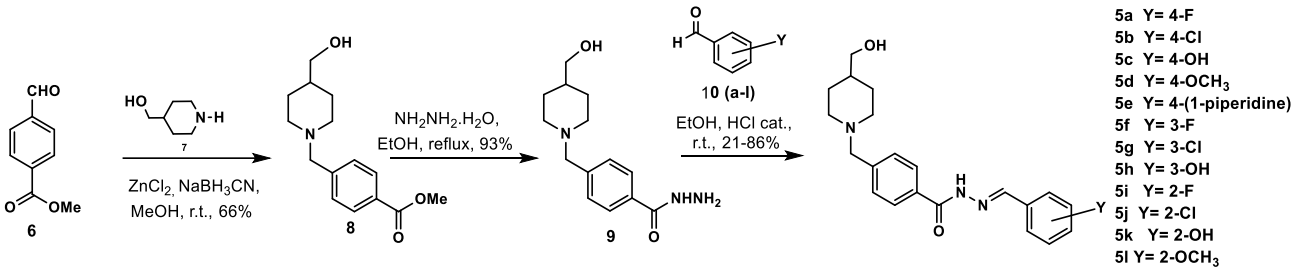

Scheme 1. Synthetic route for the synthesis of the target compounds **5a-l**.

2.2. Molecular docking

Molecular docking experiments with the inhibitor donepezil were performed into the AChE binding site to validate the three states evaluated for the enzyme (i.e. free, acetylated, and Michaelis complex). The top-ranked pose of docking experiments was compared with the experimental conformation of donepezil complexed with AChE (Protein Data Bank (PDB), code 4ey7). The docking simulation successfully found the experimental binding mode of donepezil in both free and acetylated forms, while for the Michaelis complex, the donepezil molecule adopts a completely inverted binding mode with a significantly worse score. Almost all compounds exhibited similar docking scores and binding modes in both free and acetylated forms of the AChE. The compounds were predicted to interact with the same region as donepezil in the AChE cavity but with a different profile of intermolecular interactions as exemplified for compound PQM-181 (**5k**) (Figure 2).

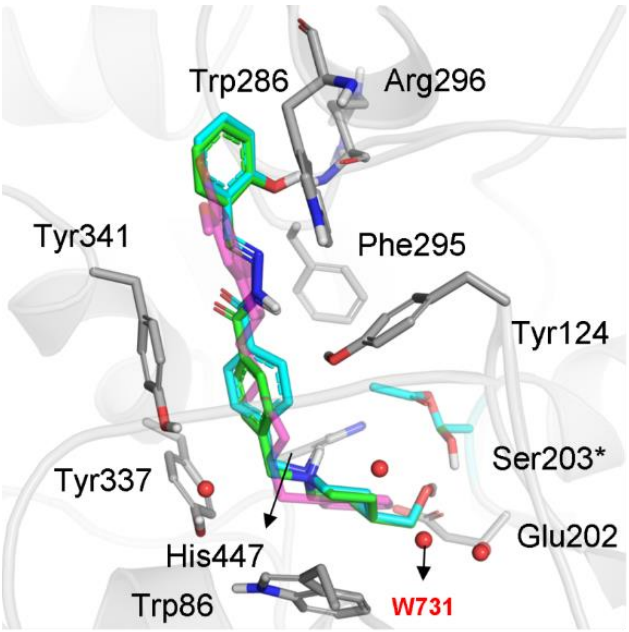

Figure 2. Docking results for PQM-181 (**5k**, Y=2-OH) in the (A) free (green) and acetylated (light blue) states. This figure was generated with Pymol (The PyMOL Molecular Graphics System, Version 2.0 Schrödinger, LLC, available at https://pymol.org/) and Inkscape (Inkscape Project, 2020, available at: https://inkscape.org).

The experimental binding mode of donepezil is represented as pink sticks, and water molecules are represented as red spheres. Ser203 residues in the free and acetylated states are highlighted with an asterisk. The overall binding mode of the tested compounds is characterized by: (i) cation-π interaction between the protonated nitrogen from the piperidinyl ring and Trp86, (ii) a hydrogen bond of the piperidine hydroxyl group with the conserved Glu202 and close polar contact with the Ser199 donor hydroxyl group of the free state, (iii) π-π stacking between the phenyl ring aromatic residues in the middle gorge, and (iv) *N*-acylhydrazone moiety hydrogen-bonded with amino acid residues in the middle of the binding cavity. The interactions (i) and (ii) are observed for all compounds, while (iii) and (iv) interactions differ according to the substituent of the phenyl ring interacting with the peripheral anionic site (PAS). According to the docking results in the free form of the enzyme, the halogen substituent is best located at the *ortho* position. On the other hand, *para* substituents are predicted to be more exposed to the solvent, while *meta* and *ortho* halogens are buried in the cavity formed by the PAS at the entrance of the gorge. These findings are shown in Figure 3 for compound PQM-179 (**5i**, Y= 2-F, docking score= -14.589 kcal mol^{-1}, Figure 3A) interacting with the Trp286 residue from PAS through a π-π stacking, while compound PQM-180 (**5j,** Y= 2-Cl, docking score= -14.829 kcal mol^{-1}, B) performs a halogen bond with the NH group from the main chain of Arg296 (4.30Å).

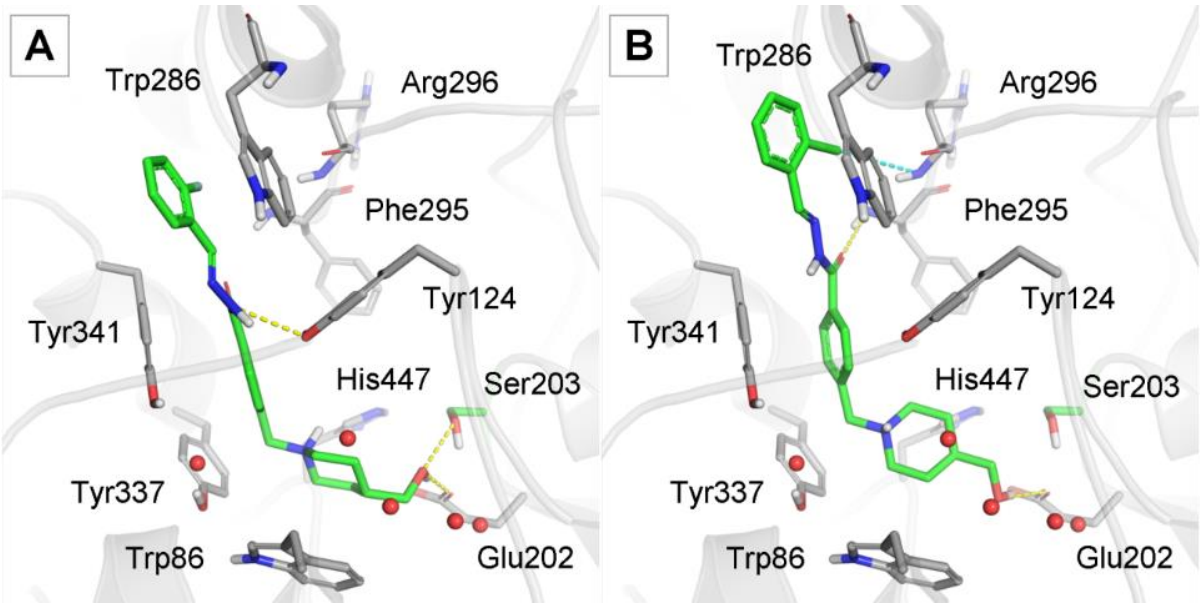

Figure 3. Docking results for compounds **5i** (A) and **5j** (B) in the free AChE. Water molecules are represented as red spheres, hydrogen and halogen bonds are represented as yellow and cyan dashes, respectively. This figure was generated with Pymol (The PyMOL Molecular Graphics System, Version 2.0 Schrödinger, LLC, available at https://pymol.org/) and Inkscape (Inkscape Project, 2020, available at: https://inkscape.org).

The insertion of the polar hydroxyl group at the phenyl ring is also most favourable at the *ortho* position (Figure 4A). In fact, compound PQM-181 (**5k**, Y= 2-OH, docking score= -16.851 kcal mol^{-1}) was predicted to be the ligand with the best affinity for AChE, being predicted as more potent than donepezil in both free and acetylated forms of the enzyme with dockings scores values of -16.851 and -16.331 kcal mol^{-1}, respectively. It seems that, at least in part, the higher affinity of compound **5k** could be due to the ability of the hydroxyl group to perform two hydrogen bonds with the same amino acid residue Arg296, donating a hydrogen bond to the carbonyl oxygen (2.74Å), while accepting another hydrogen bond from main chain NH (3.00Å) (Figure 4B).

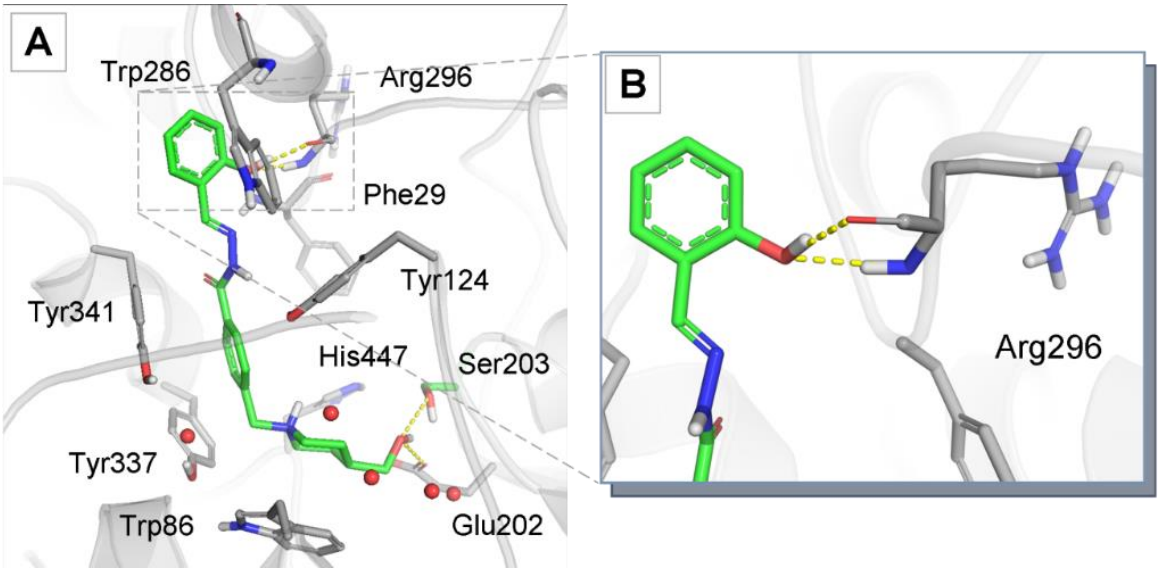

Figure 4. (A) Docking result of PQM-181 (**5k**) in the free state of AChE. (B) Interaction with Arg296 from PAS. Water molecules are represented as red spheres, and hydrogen bonds are represented as yellow dashes. This figure was generated with Pymol (The PyMOL

Molecular Graphics System, Version 2.0 Schrödinger, LLC, available at https://pymol.org/) and Inkscape (Inkscape Project, 2020, available at: https://inkscape.org).

Table 1. Docking scores of compounds **5a-l** and donepezil (used as reference) provided by docking with Glide in the Extra Precision Mode.

Compound	Substituent (Y)	Free AChE	Acetylated AChE	Michaelis Complex
PQM-170 (5a)	4-F	-14.021	-14.003	-9.020
PQM-171 (5b)	4-Cl	-14.791	-14.742	-9.445
PQM-172 (5c)	4-OH	-13.912	-14.053	-8.181
PQM-173 (5d)	4-OCH_3	-14.693	-13.662	-9.961
PQM-174 (5e)	4-(1-piperidine)	-13.391	-14.997	-9.330
PQM-175 (5f)	3-F	-14.247	-14.792	-8.756
PQM-176 (5g)	3-Cl	-14.317	-14.707	-7.924
PQM-177 (5h)	3-OH	-14.889	-14.908	-10.544
PQM-179 (5i)	2-F	-14.589	.14.673	-8.450
PQM-180 (5j)	2-Cl	-14.820	-14.962	-6.343
PQM-181 (5k)	2-OH	-16.851	-16.331	-7.961
PQM-182 (5l)	2-OCH_3	-14.501	-14.752	-7.088
Donepezil	-	-15.469	-15.862	-11.757

All compounds exhibited a significant degradation of the docking scores in the Michaelis complex, indicating that the interaction with AChE is significantly less favourable when ACh is present in the binding site. Furthermore, as expected, the *in silico* results clearly showed that the change in position and the extension in one methylene unit the substitution of the hydroxy group in the piperidine ring of compounds **5a-l** could, in fact, lead to additional H-bond interactions between the -OH group and Glu202 residue in the active site of AChE (Figure 4), and a possible enhanced inhibitory activity, which was not possible either in the original prototype **4g*S*** (Figure 5) or in the other compounds from the original 3-hydroxy-piperidine parent analogues from series **4** [24].

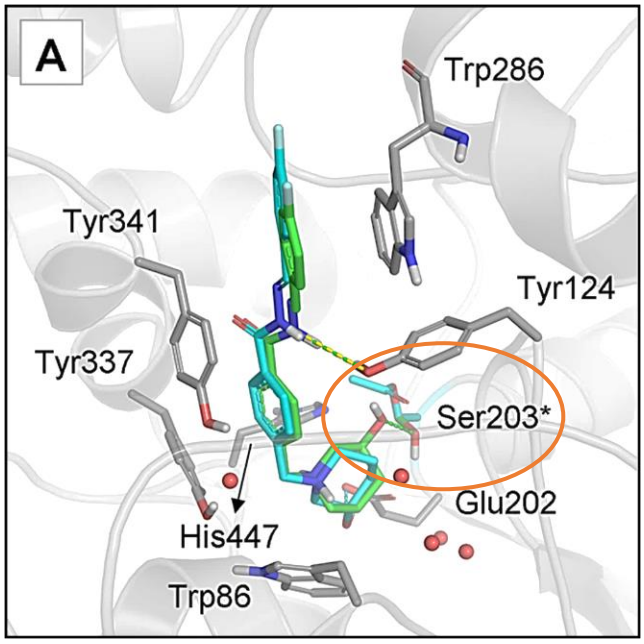

Figure 5. Docking results for the prototype ligand **4gS** in the free (green) and acetylated (light blue) states, highlighting the absence of H-bond interactions with Glu202 residue. This figure was generated with Pymol (The PyMOL Molecular Graphics System, Version 2.0 Schrödinger, LLC, available at https://pymol.org/) and Inkscape (Inkscape Project, 2020, available at: https://inkscape.org).

2.3. In Vitro Inhibition of AChE and BuChE

Compounds **5a-l** were preliminary evaluated *in vitro* for their inhibitory activity of AChE and butyrylcholinesterase (BuChE) in a fixed-dose of 30 µM. The experiment was performed twice in triplicate, according to the modified Ellman method [25], using AChE purified from *Electrophorus electricus* (EeAChE) and equine BuChE (eqBuChE). The results are shown in Figure 6.

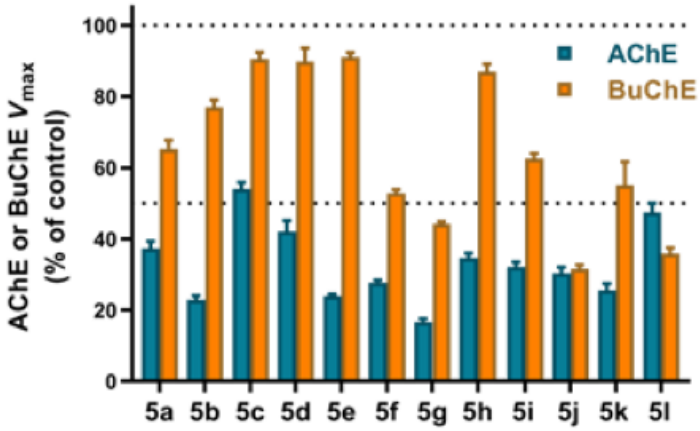

Figure 6. *In vitro* evaluation of the inhibitory activity of compounds **5a-l** (30 µM) against EeAChE and eqBuChE (bars are means ± pooled s. d. of two experiments, each in triplicate).

Almost all compounds exhibited an AChE inhibition higher than 50% at 30 µM, except for compound **5c** (~45%), with IC_{50} values ranging from 3.3 to 26.4 µM. Results from dose-response curves and selectivity against AChE and BuChE

(Table 2) revealed compounds **5b**, **5e-g**, **5j** and **5k** as the most potent and selective for AChE inhibition, especially for compounds PQM-171 (**5b,** IC_{50}= 5.6 μM), PQM-176 (**5g,** IC_{50}= 3.3 μM) and PQM-181 (**5k,** IC_{50}= 5.9 μM), that showed selectivity indexes of >5.4, 15.0 and >5.1, respectively.

Table 2. IC_{50} values and selectivity of compounds **5al** for inhibition of AChE and BuChE.

Compound	IC_{50} (μM) [a]		selectivity [b]
	AChE	BuChE	
PQM-170 (5a)	26.4	>30	>1.1
PQM-171 (5b)	**5.6**	**>30**	**>5.4**
PQM-172 (5c)	25.1	>30	>1.2
PQM-173 (5d)	15.3	>30	>2.0
PQM-174 (5e)	12.0	>30	>2.5
PQM-175 (5f)	8.2	>30	>3.6
PQM-176 (5g)	**3.3**	**49.8**	**15.0**
PQM-177 (5h)	13.9	>30	>2.2
PQM-179 (5i)	12.0	>30	>2.5
PQM-180 (5j)	9.0	12.9	1.4
PQM-181 (5k)	**5.9**	**>30**	**>5.1**
PQM-182 (5l)	13.5	12.9	1.0

[a] Geometric mean of two curves. [b] BuChE/AChE IC_{50} ratio.

The mechanism of AChE inhibition was also investigated. Among the best AChE inhibitors, compounds PQM-171 (**5b**), PQM-174 (**5e**), PQM-176 (**5g**) and PQM-181 (**5k**) were chosen for this study according to their structural attributes aiming to observe the contribution of the aromatic substitution pattern (size and nature of substituent and position) in the type of enzyme inhibition mechanism. Thus, compound **5b** (IC_{50}= 5.6 μM) with a small electron-withdrawing substituent chlorine in the *para*-position, compound **5e** (IC_{50}= 12.0 μM) with the bulky and electron-donating 1-piperidine substituent in the *para*-position, compound **5g** (IC_{50}= 3.3 μM) with a small chlorine atom at *meta*-position and compound **5k** (IC_{50}= 5.9 μM), with the small electron-donating and H-bond donator/acceptor *ortho*-hydroxy group were evaluated about the steric and regiochemical influence of the substituent in the mechanism of AChE inhibition. In Figure 7, one can observe that all four compounds reduced V_{max}, but PQM-171 (**5b**), PQM-176 (**5g**) and PQM-181 (**5k**) exhibited mixed mechanisms of enzyme inhibition, with affinity reduction factors of ternary complex formation (alpha) of 2.34 to 3.09, whereas compound **5k** seems to inhibit the enzyme by a simple non-competitive type mechanism. This difference in the mode of enzyme inhibition could be related to the ability of **5k** to perform singular H-bonds interactions with the amino acid residue Arg296, as observed in the docking studies (Figure 4B).

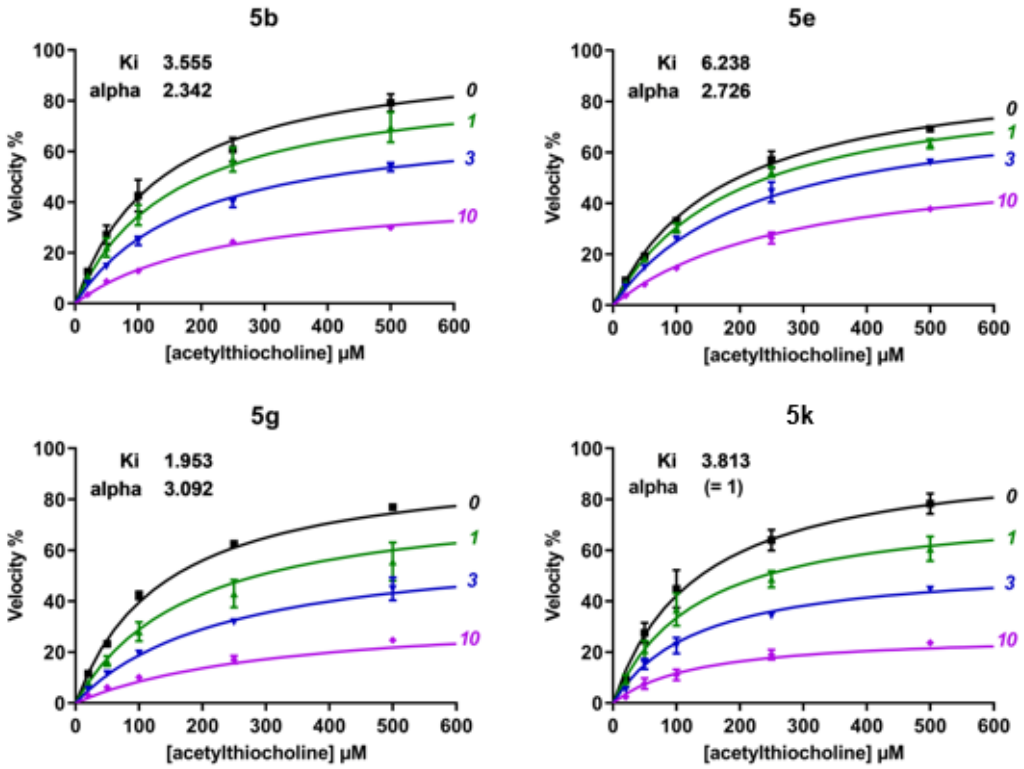

Figure 7. Mechanism of AChE inhibition of compounds **5e**, **5d**, **5g** and **5k.** The K_i (µM) and alpha factors obtained from the best-fitting models are indicated in each plot, and compound concentrations (µM) are shown near each curve (symbols are means ± s. e. m. of 2-3 experiments, each in triplicate).

2.4. In vitro cytotoxicity evaluation

The cytotoxicity of the target compounds was evaluated in human neuroblastoma (SH-SY5Y) cells and human intestinal epithelial HT-29 cells by MTT and calcein/propidium iodide assay [25], respectively. The treatment of SH-SY5Y cells with concentrations up to 40 µM of compounds PQM-171(**5b**) and PQM-176 (**5g**) for 24h did not affect neuronal viability. In similar treatment time, compounds PQM-174 (**5e**) and PQM-181 (**5k**) reduced neuronal viability at 20 µM ,40 µM and 80 µM (Supplementary information, Fig. S1). In parallel, epithelial HT-29 cells treated with concentrations up to 30 µM of the studied compounds **5a**–**l** for 24h did not show any cytotoxicity (data not shown). Therefore, we selected the range of 0.625 – 10 µM to evaluate the antioxidant activity of compounds **5b**, **5g** and **5k** in neuronal SH-SY5Y cells.

2.5. In silico and in vitro druggability assessments

ADMET parameters were predicted in silico by using the QikProp v. 3.5 (Schrödinger). Our data indicate that the most promising multifunctional compounds PQM-171 (**5b**), PQM-176 (**5g**) and PQM181 (**5k**) are in accordance with the software reference parameters (Table 3) and compared to donepezil, with adequate clogP and water solubility, good predicted serum albumin binding, human absorption and blood-brain barrier transposition. Moreover, none of the highlighted compounds contravenes Lipinski's rule of druggability.

Table 3: *In silico* ADMET prediction data for compounds **5a-l**.

Compound	MW	QPlog Po/w	HBA	HBD	PSA	% HOA	QPlogS	QPPCaco	QPlogBB
PQM-170 (5a)	369.4	3.387	6.2	2	73.15	88.04	-4.28	202.03	-0.62
PQM-171 (5b)	**385.9**	**3.702**	**6.2**	**2**	**74.59**	**89.59**	**-4.87**	**194.60**	**-0.62**
PQM-172 (5c)	367.4	2.556	6.95	3	98.66	73.63	-4.02	59.14	-1.46
PQM-173 (5d)	381.5	3.256	6.95	2	83.62	85.90	-4.27	169.31	-0.91
PQM-174 (5e)	434.6	4.240	7.2	2	77.20	91.94	-5.81	175.57	-0.89
PQM-175 (5f)	369.4	3.448	6.2	2	74.51	88.16	-4.49	195.96	-0.66
PQM-176 (5g)	**385.9**	**3.749**	**6.2**	**2**	**75.92**	**89.94**	**-4.91**	**196.49**	**-0.62**
PQM-177 (5h)	367.4	2.559	6.95	3	99.55	73.52	-4.07	58.22	-1.48
PQM-179 (5i)	369.4	3.455	6.2	2	75.92	88.20	-4.46	195.96	-0.68
PQM-180 (5j)	385.9	3.691	6.2	2	76.00	89.54	-4.78	194.79	-0.63
PQM-181 (5k)	**367.4**	**2.566**	**6.95**	**3**	**96.81**	**75.23**	**-3.84**	**72.21**	**-1.33**
PQM-182 (5l)	381.5	3.435	6.95	2	82.19	88.22	-4.66	199.45	-0.88
donepezil	379.49	4.442	5.5	0	46.289	100	-4.63	894.51	0.12

QPlogP o/w-Predicted octanol/water partition coefficient (-2.0 to 6.5). **HBA**-Hydrogen bonding acceptors (2 to 20). **HBD**-Hydrogen bonding donor (0 to 6). **PSA**-Van der Waals surface area of polar nitrogen and oxygen atoms (7 to 200). **% HOA**-Percentage of human absorption by oral route (<25%-low; >80%-high). **QPlogS**-Aqueous solubility (-6.5 to 0.5); **QPPCaco**-Permeability in Caco cell assay, model for intestinal absorption (<25–low; >500–high); **QPlogBB**-Permeability in the blood-brain barrier (-3.0 to 1.2).

2.6. In vitro antioxidant activity

As discussed earlier, OS plays a central role in the clinical development of AD. In order to explore the multi-target activity profile of the most promising compounds from the series **5**, neuronal SH-SY5Y cells were incubated for 30 min with different concentrations (0.625-10 µM) of compounds PQM-171 (**5b**), PQM-176 (**5g**) and PQM-181 (**5k**) in the presence of *tert*-butyl hydroperoxide (*t*-BOOH, 100 µM). *t*-BOOH is known to generate ROS from lipid peroxidation in different brain regions [26]. The intracellular ROS formation was therefore detected by using the fluorescent probe 2,7-dichlorodihydrofluorescein diacetate (H_2DCF-DA). As shown in figure 8, compound PQM-181 (5k) inhibited the ROS formation at 2.5 µM, 5 µM and 10 µM, while compounds PQM-171 (5b) and PQM-176 (5g) inhibited the ROS formation only at 10 µM. Among these compounds, **5k** exhibited the highest antioxidant activity with an IC_{50} value of 7.45 µM and a maximum inhibition percentage of 67.14 % at 10 µM (Table 4). Based on these results, we selected compound **5k** to evaluate its potential neuroprotective effect against *t*-BOOH and oligomers of $A\beta_{1-42}$ peptide ($OA\beta_{1-42}$).

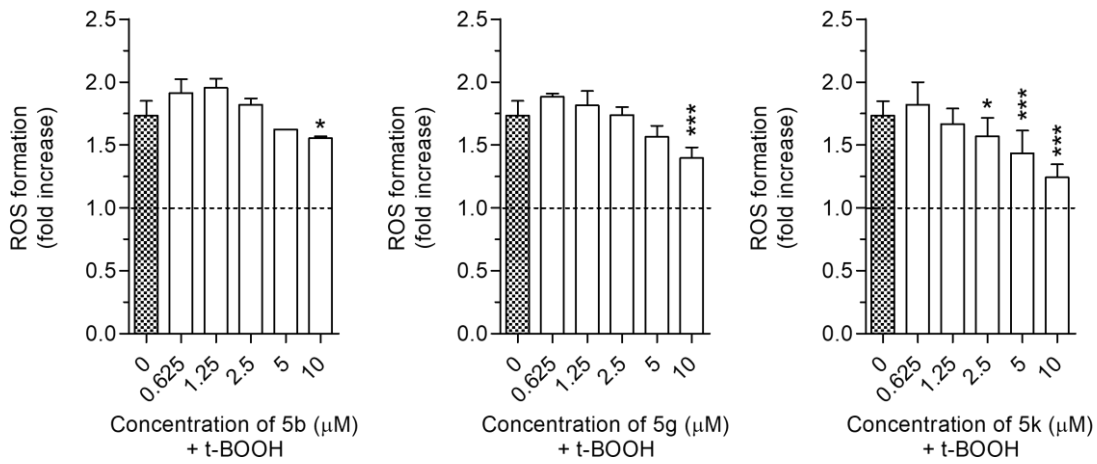

Figure 8. Compounds 5b, 5g and 5k inhibit the ROS formation induced by *t*-BOOH in SH-SY5Y cells. Cells were incubated for 30 min with various concentrations of compounds **5b**, **5g** and **5k** (0.625 – 10 μM) in the presence of *t*-BOOH (100 μM). At the end of incubation, the ROS formation was detected by using the fluorescent probe H_2DCF-DA as described in the materials and methods section. Data are expressed as fold increase and reported as mean ± SD of three independent experiments (*p<0.05 and ***p<0.001 vs cells treated with *t*-BOOH at one-way ANOVA with Dunnett post hoc test).

Table 4. Antioxidant activity of compounds **5b**, **5g** and **5k** in neuronal SH-SY5Y cells treated with *t*-BOOH (100 μM).

Compound	% Inhibition (10 μM)	IC_{50} (μM)
PQM-171 (5b)	24.49 ± 1.66	-
PQM-176 (5g)	45.96 ± 0.32	-
PQM-181 (5k)	67.14 ± 3.31	7.45

In vitro neuroprotective activity

The neuroprotective activity of compound PQM-181 (**5k**) against the neurotoxicity evoked by *t*-BOOH and OAβ_{1-42} was evaluated in neuronal SH-SY5Y cells using MTT assay. In particular, cells were incubated for 4 h with various concentrations of compound **5k** (2.5 - 10 μM) in the presence of either *t*-BOOH (50 μM) or OAβ_{1-42} (10 μM). As shown in figure 9, compound **5k** significantly counteracts the neurotoxicity induced by *t*-BOOH and OAβ_{1-42} at all the concentrations used. Based on these findings, we also evaluated the effects of **5k** on Aβ_{1-42} aggregates by the thioflavin fluorescence assay. Our results evidenced a moderate activity of compound **5k** in the disaggregation of Aβ_{1-42} aggregates with a maximum anti-amyloidogenic activity of 30% at 75 μM. (supplementary material, figure 49).

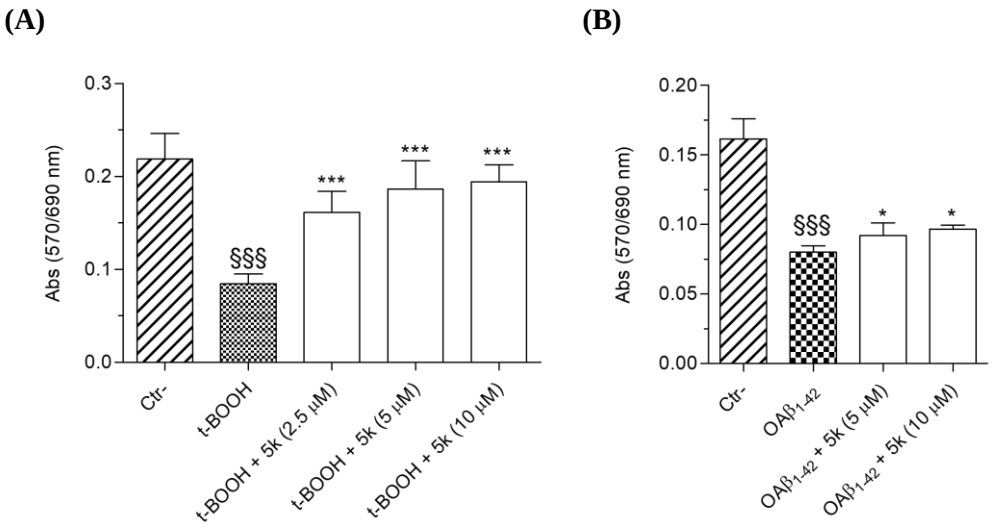

Figure 9. Neuroprotective activity of compound **5k** against the neurotoxicity induced by either *t*-BOOH or $A\beta_{1-42}$ in SH-SY5Y cells. Cells were incubated for 4 h with various concentrations of compound **5k** (2.5 – 10 µM) in the presence of either *t*-BOOH (50 µM) **(A)** or $OA\beta_{1-42}$ (10 µM) **(B)**. Data are expressed as absorbance (Abs) and reported as mean ± SD of three independent experiments (§§§$p<0.001$ vs untreated cells, *$p<0.05$ and ***$p<0.001$ vs cells treated with *t*-BOOH or $OA\beta_{1-42}$ at one-way ANOVA with Bonferroni post hoc test).

3. Experimental section

3.1. Chemistry

Reagents were obtained from Sigma-Aldrich, ACROS or Merck. The solvents were prepared by standard procedures. Analytical thin-layer chromatography (TLC) was performed using silica 60 F254 from Merck, and spots were visualized with UV light. Melting points were measured in capillary tubes on a Marte (PFM II) melting point apparatus without correction. Nuclear magnetic resonance (NMR) spectroscopy was performed on a Bruker AC-300 NMR (tetramethylsilane (TMS) used as internal standard). Chemical shifts were reported in parts per million (ppm) downfield from TMS. Proton coupling patterns were described as singlet (s), doublet (d), triplet (t), quartet (q), multiplet (m), doublet of quartets (dq) and triplet of doublets (td). High-resolution mass spectra (HRMS) were obtained by electrospray ionization (ESI) using an Agilent 6550 iFunnel Q-TOF LC/MS. Infrared (IR) spectra were obtained by Nicolet iS50 FTIR (Thermo Scientific USA) infrared spectrometer coupled to Pike Gladi ATR Technologies. The absorption bands were reported in wavenumbers (cm^{-1}). All spectra are available in supporting information.

*Methyl 4-((4-(hydroxymethyl)piperidin-1-yl)methyl)benzoate (**8**)*

In a flask was added the compounds methyl 4-formylbenzoate (0.59 g, 3.62 mmol), (piperidin-4-yl)methanol (0.5 g, 4.34 mmol), zinc chloride (0.25 g, 1.81 mmol) and sodium cyanoborohydride (0.23 g, 3.62 mmol) in methanol (10 mL). The resultant mixture was stirred at room temperature for 5 h. The solvent was evaporated and water was added (10 mL), followed by addition of a solution of NaOH 20% to alkalize the mixture. Then, the mixture was extracted with CH_2Cl_2

(6x10 mL). The organic layer was separated and dried over brine and $MgSO_4$. Removal of the solvents produced a residue which was purified using column chromatography, eluted with a mixture of Ethyl acetate/MeOH (8:2, v/v), to afford compound **8** as a white solid. 66% yield. ^{1}H NMR ($CDCl_3$, 300 MHz): δ 7.94 (d, 2H, *J*=8.3), 7.36 (d, 2H, *J*=8.3), 3.87 (s, 3H), 3.50 (s, 2H), 3.45 (d, 2H, *J*=6.4), 2.84 (d, 2H, *J*=11.5), 1.99-1.93 (m, 2H), 1.67 (d, 2H, *J*=13.8), 1.54-1.37 (m, 1H), 1.25 (dq, 2H, *J*= 3.8, 12.1 e 24.2). ^{13}C NMR ($CDCl_3$, 75 MHz): 167.1, 144.1, 129.5, 129.0, 128.9, 67.8, 63.1, 53.5, 52.0, 35.5, 28.8. IR: v 3390, 3059, 3003, 2936, 2754, 1716, 1609, 1436, 1274, 1040, 753, 696.

*4-((4-(hydroxymethyl)piperidin-1-yl)methyl)benzohydrazide (**9**)*

To a solution of methyl 4-((4-(hydroxymethyl)piperidin-1-yl)methyl)benzoate (**8**, 0.5 g, 1.9 mmol) in ethanol (8 mL) was added hydrazine monohydrate (2.77 mL, 57.0 mmol). The resulting mixture was refluxed and stirred for 4 h. Removal of the solvent produced a residue which was purified by chromatography column, eluted with a mixture of EtOAc/MeOH (7:3, v/v) to afford compound **9** as a white solid. 93% yield. ^{1}H NMR (DMSO-d_6, 300 MHz): δ 6.95 (d, 2H, *J*=8.3), 6.62 (d, 2H, *J*=8.3), 2.77 (s, 2H), 2.58 (d, 2H, *J*=6.3), 2.10 (d, 2H, *J*=11.7), 1.24 (td, 2H, *J*=2.3 e 11.8), 0.92 (d, 2H, *J*=12.7), 0.74-0.57 (m, 1H), 0.45 (dq, 2H, *J*=3.1, 11.8 e 14.4). ^{13}C NMR (DMSO-d_6, 75 MHz): 159.9, 133.0, 123.8, 121.4, 118.7, 58.3, 54.3, 44.9, 30.0, 20.0. IR: v 3300, 3260, 3170, 2939, 2769, 1620, 1570, 1502, 849, 785.

*General method for the preparation of N-acylhydrazones intermediates (**5a-l**)*

To a solution of 4-((4-(hydroxymethyl)piperidin-1-yl)methyl)benzohydrazide (**9**, 0.2 g, 0.76 mmol) in ethanol with a catalytic amount of concentrated HCl was added the corresponding aldehyde (**10**, 0.912 mmol). The reaction mixture was then stirred for 5 to 12 h at room temperature, according to the used benzaldehyde. Removal of the solvent produced a residue, which was purified using recrystallization or chromatography column with the appropriate eluents systems.

*(E)-N'-(4-fluorobenzylidene)-4-((4-(hydroxymethyl)piperidin-1-yl)methyl)benzohydrazide (PQM-170, **5a**).* White solid. 21% yield. Mp 190-194 °C. ^{1}H NMR (DMSO-d_6, 300 MHz): *δ* 8.50 (s, 1H), 7,88 (d, 2H, *J*=8,0), 7.83-7.74 (m, 2H), 7.42 (d, 2H, *J*=8.1), 7.28 (t, 2H, *J*=8.8), 3.23 (d, 2H, *J*=6.2), 2.77 (d, 2H, *J*=11.2), 1.91 (t, 2H, *J*=10.6), 1.60 (d, 2H, *J*=10.8), 1.41-1.24 (m, 1H), 1.12 (dq, 2H, *J*=4.2, 12.9 e 15.9). ^{13}C NMR (DMSO-d_6, 75 MHz): *δ* 163.5, 163.3 (d, *J*=246.6), 145.0, 143.0, 131.9, 131.12, 129.5 (d, *J*=7.5), 129.0, 127.8, 116.1 (d, *J*=21.8), 66.1, 62.2, 53.4, 38.4, 28.8. IR: *v* 3406, 3024, 2918, 2854, 1655, 1566, 1287, 1232 1602. HRMS (ESI) *m/z* calcd. $C_{21}H_{25}FN_3O_2$ [M+H$^+$]: 370.1931, found 370.1918.

*(E)-N'-(4-chlorobenzylidene)-4-((4-(hydroxymethyl)piperidin-1-yl)methyl)benzohydrazide (PQM-171, **5b**).* Yellow solid. 86% yield. Mp 207-210 °C. ^{1}H NMR (DMSO-d_6, 300 MHz): *δ* 12.20 (s, 1H), 8.59 (s, 1H), 7.99 (d, 2H, *J*=7.9), 7.75 (d, 2H, *J*=8.4), 7.67 (d, 2H, *J*=7.8), 7.52 (d, 2H, *J*=8.4), 4.05 (s, 2H), 3.25 (d, 2H, *J*=5.6), 3.10 (d, 2H, *J*=10.1), 2.63-254 (m, 2H), 1.74 (d, 2H, *J*=12.0), 1.63-1.47 (m, 1H), 1.45-1.32 (m, 2H). ^{13}C NMR (DMSO-d_6, 75 MHz): *δ* 162.8, 146.7, 134.5, 133.3, 133.2, 130.5, 129.0, 128.7, 127.9, 65.1, 59.5, 51.7, 36.7, 26.5. IR: *v* 3305, 3052, 3028, 2930, 2717, 1644, 1088. HRMS (ESI) *m/z* calcd. $C_{21}H_{25}ClN_3O_2$ [M+H$^+$]: 386.1635, found 386.1627.

(E)-N'-(4-hydroxybenzylidene)-4-((4-(hydroxymethyl)piperidin-1-yl)methyl)benzohydrazide (PQM-172, ***5c****)*. Yellow solid. 21% yield. Mp 225-230 °C. ^{1}H NMR (DMSO-d_6, 300 MHz): δ 11.79 (s, 1H), 8.39 (s, 1H), 7.88 (d, 2H, *J*=8.1), 7.56 (d, 2H, *J*=8.6), 7.48 (d, 2H, *J*=8.1), 6.84 (d, 2H, *J*=8.5), 3.23 (d, 2H, *J*=6.1), 2.92 (t, 2H, *J*=16.0), 2.14 (t, 2H, *J*=10.9), 1.65 (d, 2H, *J*=11.7), 1.50-1.33 (m, 1H), 1.20 (dq, 2H, *J*=12.1 e 20.7).^{13}C NMR (DMSO-d_6, 75 MHz): δ 163.2, 159.7, 148.6, 140.6, 132.7, 129.7, 129.2, 127.8, 125.5, 116.0, 65.9, 61.4, 52.8, 37.8, 28.0. IR: *v* 3250, 2929, 1644, 1601, 1281. HRMS (ESI) *m/z* calcd. $C_{21}H_{26}N_3O_3$ [M+H$^+$]: 368.1974, found 368.1959.

(E)-N'-(4-methoxybenzylidene)-4-((4-(hydroxymethyl)piperidin-1-yl)methyl)benzohydrazide (PQM-173, ***5d****)*. Yellow solid. 37% yield. Mp 146-149 °C. ^{1}H NMR (CD_3OD, 300 MHz): δ 8.36 (s, 1H), 8.04 (d, 2H, *J*=7.8), 7.77 (d, 2H, *J*=8.0), 7.72 (d, 2H, *J*=7.8), 6.98 (d, 2H, *J*=8.2), 4.40 (s, 2H), 3.83 (s, 3H), 3.52 (d, 2H, *J*=11.0), 3.43 (d, 2H, *J*=5.5), 3.06 (t, 2H, *J*=12.0), 1.98 (d, 2H, *J*=14.8), 1.85-1.69 (m, 1H), 1.63-1.46 (m, 2H).^{13}C NMR (CD_3OD, 75 MHz): δ 164.5, 162.0, 149.9, 134.5, 133.0, 131.5, 129.2, 128.2, 126.5, 113.9, 65.1, 59.7, 54.6, 52.4, 36.0, 25.9. IR: *v* 3343, 3219, 3004, 2925, 1651, 1249. HRMS (ESI) *m/z* calcd. $C_{22}H_{28}N_3O_3$ [M+H$^+$]: 382.2131, found 382.2122.

(E)-N'-(4-(piperidin-1-yl)benzylidene)-4-((4-(hydroxymethyl)piperidin-1-yl)methyl)benzohydrazide (PQM-174, ***5e****)*. Yellow solid. 37% yield. Mp 205-208 °C. ^{1}H NMR (DMSO-d_6, 300 MHz): δ 11.58 (s, 1H), 8.30 (s, 1H), 7.84 (d, 2H, *J*=7.7), 7.52 (d, 2H, *J*=8.6), 7.44 (d, 2H, *J*=7.7), 6.95 (d, 2H, *J*=8.9), 3,60 (s, 1H), 3.28-3.20 (m, 6H), 2.93-2.80 (m, 2H), 2.28-1.94 (m, 2H), 1.68-1.50 (m, 8H), 1.42-1.29 (m, 1H), 1.25-0.82 (m, 2H).^{13}C NMR (DMSO-d_6, 75 MHz): δ 162.5, 152.5, 148.3, 132.7, 129.5, 128.9, 128.0, 123.4, 114.7, 65.8, 61.6, 52.9, 48.7, 38.0, 28.3, 25.0, 24.4. IR: *v* 3346, 29,23, 1643, 1276. HRMS (ESI) *m/z* calcd. $C_{26}H_{35}N_4O_2$ [M+H$^+$]: 435.2760, found 435.2765.

(E)-N'-(3-fluorobenzylidene)-4-((4-(hydroxymethyl)piperidin-1-yl)methyl)benzohydrazide (PQM-175, ***5f****)*. Yellow solid. 47% yield. Mp 134-138 °C. ^{1}H NMR (C_5D_5N, 300 MHz): δ 13.09 (s, 1H), 9.07 (s, 1H), 8.56-8.32 (m, 2H), 8.06-7.87 (m, 2H), 7.85-7.72 (m, 1H), 7.43-7.24 (m, 2H), 7.16-7.01 (m, 1H), 4.16 (s, 2H), 3.81-3.63 (m, 2H), 3.48-3.20 (m, 2H), 2.73-2.53 (m, 2H), 2.15-1.92 (m, 4H), 1.90-1.70 (m, 1H). ^{13}C NMR (C_5D_5N, 75 MHz): δ 164.3, 163.1(d, *J*=244.5), 146.9, 137.8, 136.7, 134.5, 131.1, 130.6 (d, *J*=7.8), 128.6, 116.7 (d, *J*=21.0), 113.5 (d, *J*=21.0), 66.0, 60.5, 52.4, 36.7, 27.0. IR: *v* 3340, 1651, 1548, 1270, 1129. HRMS (ESI) *m/z* calcd. $C_{21}H_{25}FN_3O_2$ [M+H$^+$]: 370.1931, found 370.1918.

(E)-N'-(3-chlorobenzylidene)-4-((4-(hydroxymethyl)piperidin-1-yl)methyl)benzohydrazide (PQM-176, ***5g****)*. Gray solid. 59% yield. Mp 199-204 °C. ^{1}H NMR (C_5D_5N, 300 MHz): δ 12.91 (s, 1H), 8.82 (s, 1H), 8.52-7.62 (m, 5H), 7.42-7.21 (m, 3H), 4.00-3.50 (m, 4H), 2.83-2.24 (m, 2H), 2.45-2.07 (m, 2H), 1.95-1.64 (m, 4H), 1.37-1.14 (m, 1H). ^{13}C NMR (C_5D_5N, 75 MHz): δ 164.5, 146.3, 137.3, 134.6, 133.8, 130.3, 130.0, 129.7, 128.4, 127.0, 125.9, 66.5, 61.6, 53.1, 35.5, 28.1. IR: *v* 3323, 3033, 3011, 2926, 2871, 1651, 1270, 1038. HRMS (ESI) *m/z* calcd. $C_{21}H_{25}ClN_3O_2$ [M+H$^+$]: 386.1635, found 386.1627.

(E)-N'-(3-hydroxybenzylidene)-4-((4-(hydroxymethyl)piperidin-1-yl)methyl)benzohydrazide (PQM-177, ***5h****)*. Yellow solid. 35% yield. Mp 163-167 °C. ^{1}H NMR (CD_3OD, 300 MHz): δ 8.33 (s, 1H), 8.00 (d, 2H, *J*=8.2), 7.64 (d, 2H, *J*=8.2), 7.30 (s, 1H), 7.24 (d, 2H, *J*=6.3), 6.87 (m, 1H), 4.14 (s, 2H), 3.43 (d, 2H, *J*=6.1), 2.74 (t, 2H, *J*=11.6), 2.74 (d, 2H, *J*=12.7), 1.75-1.60 (m, 1H), 1.57-1.40 (m, 2H). ^{13}C NMR (CD_3OD, 75 MHz): δ 164.9, 157.6, 149.8, 136.0, 135.3, 133.4, 130.8, 129.5, 128.0, 119.4, 117.7, 113.1, 65.4, 30.3, 52.4, 36.6, 26.4. IR: *v* 3345, 2933, 1644, 1281. HRMS (ESI) *m/z* calcd. $C_{21}H_{26}N_3O_3$ [M+H$^+$]: 368.1974, found 368.1959.

(E)-N'-(4-fluorobenzylidene)-4-((4-(hydroxymethyl)piperidin-1-yl)methyl)benzohydrazide (PQM-179, ***5i****)*. Pale yellow solid. 60% yield. Mp 129-132 °C. ^{1}H NMR (CD_3OD, 300 MHz): δ 8.69 (s, 1H), 8.17 (td, 1H, *J*=1.5 e 7.7), 8.03 (d, 2H, *J*=8.2), 7.68 (d, 2H, *J*=8.3), 7.50-7.42 (m, 1H), 7.28-7.12 (m, 2H), 4.22 (s, 2H), 3.44 (d, 2H, *J*=6.2), 3.36 (d, 2H, *J*=12.1), 2.84 (t, 2H, *J*=11.5), 1.92 (d, 2H, *J*=13.8), 1.81-1.63 (m, 1H), 1.59-1.44 (m, 2H). ^{13}C NMR (CD_3OD, 75 MHz): δ 164.9, 161.7 (d, *J*=250.9, 142.4, 135.3, 133.5, 132.2 (d, *J*=8.7), 131.0, 128.1, 126.8, 124.4 (d, *J*=2.8), 121.7 (d, *J*=9.7), 115.4 (d, *J*=21.2), 65.3, 60.0, 52.3, 36.4, 26.2. IR: *v* 3331, 1651, 1614, 1286, 850, 805, 755. HRMS (ESI) *m/z* calcd. $C_{21}H_{25}FN_3O_2$ [M+H$^+$]: 370.1931, found 370.1918.

(E)-N'-(2-chlorobenzylidene)-4-((4-(hydroxymethyl)piperidin-1-yl)methyl)benzohydrazide (PQM-180, ***5j****)*. White solid. 34% yield. Mp 190-194 °C. ^{1}H NMR (C_5D_5N, 300 MHz): δ 12.95 (s, 1H), 9.22 (s, 1H), 8.55-8.38 (m, 1H), 8.34 (d, 2H, *J*=7.6), 7.67-7.63 (m, 2H), 7.43-7.34 (m, 1H), 7.30-7.26 (m, 2H), 3.78-3.67 (m, 4H), 3.05 (d, 2H, *J*=10.2), 2.21 (t, 2H, *J*=10.8), 1.94-1.85 (m, 2H), 1.79-1.65. ^{13}C NMR (C_5D_5N, 75 MHz): δ 164.5, 143.9, 141.1, 134.1, 133.6, 132.4, 131.1, 129.9, 128.30, 127.5, 127.3, 66.6, 61.9, 53.2, 36.8, 28.4. IR: *v* 3380, 3218, 3064, 2912, 1647, 1547, 1284. HRMS (ESI) *m/z* calcd. $C_{21}H_{25}ClN_3O_2$ [M+H$^+$]: 386.1635, found 386.1627.

(E)-N'-(2-hydroxybenzylidene)-4-((4-(hydroxymethyl)piperidin-1-yl)methyl)benzohydrazide (PQM-181, ***5k****)*. Pale yellow solid. 57% yield. Mp 180-184 °C. ^{1}H NMR (DMSO-d_6, 300 MHz): δ 12.38 (s, 1H), 8.74 (s, 1H), 8.03 (d, 2H, *J*=8.2), 7.76 (d, 2H, *J*=8.1), 7.52 (d, 1H, *J*=7.6), 7.25-7.33 (m, 1H), 6.96-6.88 (m, 2H), 3.35 -3.20 (m, 6H), 2.85-2.97 (m, 2H), 1.79 (d, 2H, *J*=12.3), 1.62-1.40. ^{13}C NMR (DMSO-d_6, 75 MHz): δ 162.8, 157.9, 149.1, 134.1, 134.0, 132.0, 129.9, 128.5, 119.9, 119.1, 116.9, 65.3, 59.0, 51.9, 36.4, 26.1. IR: *v* 3336, 3039, 2929, 1674, 1278. HRMS (ESI) *m/z* calcd. $C_{21}H_{26}N_3O_3$ [M+H$^+$]: 368.1974, found 368.1959.

(E)-N'-(2-methoxybenzylidene)-4-((4-(hydroxymethyl)piperidin-1-yl)methyl)benzohydrazide (PQM-182, ***5l****)*. Yellow solid. 57% yield. Mp 133-138 °C. ^{1}H NMR (C_5D_5N, 300 MHz): δ 12.83 (s, 1H), 9.38 (s, 1H), 8.46-8.22 (m, 3H), 7.96 (d, 2H, *J*=7.1), 7.29 (t, 1H, *J*=7.4), 6.94 (t, 1H, *J*=7.2), 6.85 (d, 1H, *J*=7.9), 4.30 (s, 2H), 3.64 (d, 2H, *J*=5.6) 3.59 (s, 3H), 3.40 (d, 2H, *J*=10.1), 2.79 (t, 2H, *J*=10.3), 2.17-2.01 (m, 2H), 1.94 (d, 2H, *J*=13.4), 1,87-1,76. ^{13}C NMR (DMSO-d_6, 75 MHz): δ 163.1, 158.3, 143.9, 133.6, 132.1, 136.7, 128.2, 126.0, 122.7, 121.2, 120.4, 112.3, 65.6, 60.4, 56.2, 52.5, 37.3, 27.2. IR: *v* 3358, 2934, 16511, 1249. HRMS (ESI) *m/z* calcd. $C_{22}H_{28}N_3O_3$ [M+H$^+$]: 382.2131, found 382.2122.

3.2. Molecular docking of AChE inhibition

Three different states of AChE were considered: the free and acetylated enzyme as well as the Michaelis complex (AChE complexed with the substrate ACh). All models were based on the structure of the AChE complexed with the potent inhibitor donepezil at the resolution of 2.35Å (PDB code 4EY7) [27]. We generated the acetylated model from the X-ray structure of AChE-donepezil (PDB code 4EY7) since this inhibitor is proposed to inhibit the enzyme on both free and acetylated forms[28]. Four water molecules W729, W722, W731, W737 and W931 were extracted from the structure of the AChE complexed with donepezil (PDB code 4EY7) and considered explicitly during the docking experiments. Docking studies were performed with the Glide software (version 6.2, Schrödinger, LLC, New York, NY, 2014) using the Extra Precision Docking mode [29] and the coordinate centre based on the native ligand present in the 4EY7 complex (X: 9.6, Y: -6.7 and Z: -35.73). Only the top ranked pose for each configuration of each compound (according to the XP Pose Rank) was maintained for the analyses.

3.3. In vitro studies

3.3.1 AChE and BuChE inhibition in vitro

Enzyme activity of EeAChE (E.C. 3.1.1.7, type V-S, purified from *Electrophorus electricus*) and eqBuChE (E.C. 3.1.1.8, purified from equine serum) was assayed kinetically by Ellman's method [30] in 96-well plates, as previously described [25,31], with minor modifications. Compound samples were dissolved at 0.05 M in DMSO and diluted in sodium phosphate buffer (SPB, 0.1 M, pH 7.4) immediately before use (final DMSO less than 0.2% v.v.). All other assay reagents were dissolved in SPB. The final assay volume was 200 μL; three wells were used per condition in each experiment. Sequential additions were: 20 μL of enzyme (0.5 U/mL), 5 μL of 5,5'-dithiobis-(2-nitrobenzoic) acid (10 mM), 100 μL of compound solution (twice the final concentration) and 55 μL of SPB. After ten minutes of incubation, 20 μL of the substrate (acetylthiocholine or butyrylthiocholine iodide, 0.5 M final, or 0.02-0.5 M for the competition experiments) were added, and absorbance was read in a SpectraMax 250 spectrophotometer (Molecular Devices) at 412 nm every 12 s, for 5 min at rt. Progression curves were acquired through SOFTmax PRO 5.0 (Molecular Devices), from which maximum hydrolysis velocity was estimated and analysis performed with Prism (Graphpad). Two six-point inhibition curves were obtained independently for each compound for estimation of average IC_{50}. The substrate competition data from 2-3 experiments were pooled and analyzed by global nonlinear fitting of standard kinetic models [31]. Because all compounds clearly reduced EeAChE V_{max}, only simple (pure) non-competitive and linear mixed inhibition models were fitted, being then compared and selected by likelihood criteria (corrected Akaike information criterion). All chemicals were purchased from Sigma-Aldrich (Brazil).

3.3.2 Cell cultures

Human neuronal SH-SY5Y and human intestinal epithelial HT-29 cells were routinely grown in Dulbecco's modified Eagle's Medium and Ham's F10, respectively, supplemented with 10% fetal bovine serum, 2 mM L-glutamine, 50 U/mL penicillin and 50 µg/mL streptomycin at 37 °C in a humidified incubator with 5 % CO_2.

3.3.3 Determination of cytotoxicity

Neuronal viability was assessed by the MTT (3- (4,5-dimethyl-2-thiazolyl) -2,5-diphenyl-2H-tetrazolium bromide) assay as previously described [32]. Cells were seeded in a 96-well plate at 2 x 10^4 cells/well, incubated for 24 h and then treated for 24 h with the studied compounds **5b**, **5e, 5g** and **5k** at various concentrations (2.5 - 80 µM). At the end of incubation, the MTT solution (5 mg/mL) in Hank's balanced salt solution (HBSS) was added for 2 h at 37 °C in 5% CO_2. After washing with HBSS, the formazan crystals were dissolved in 150 µL of isopropanol. The amount of formazan was measured (570 nm, filter reference 690 nm) using a microplate reader (VICTOR™ X3, Perkin Elmer, Waltham, MA, USA).

The viability of intestinal epithelial cells was determined by calcein/propidium iodide assay [14]. Cells were cultured in 96-well plates at 70% confluency, then compounds were added (30 µM final) and incubated for 24 h. The cells were then incubated with calcein AM 0.1 µM and propidium iodide 7.5 µM for 20 minutes, and fluorescence was read with a Flexstation III reader (Molecular Devices, 9×9 readings per well). Cells in positive (digitonin 0.05% w/v) and negative (vehicle) control wells were further imaged for quality control. Data from independent experiments were expressed as % viable cells, according to standard Live/Dead protocols, and pooled.

3.3.4 Determination of intracellular ROS formation

The ROS formation was assessed by using the fluorescent probe 2'-7'-dichlorohydrofluorescin diacetate fluorescent probe (H_2DCF-DA), as previously described [33]. SH-SY5Y cells were seeded in a 96-well plate at 3 x 10^4 cell/well and incubated for 24 h. Then, the culture medium was removed, and 100 µL of H_2DCF-DA (10 µg/mL) was added to each well and kept at room temperature for 30 min. At the end of incubation, cells were treated for 30 min with various concentrations (0.625 – 10 µM) of the studied compounds **5b**, **5g** and **5k** and *t*-BOOH (100 µM), simultaneously. The ROS formation was measured (excitation at 485 nm and emission at 535 nm) using a microplate reader (VICTOR™ X3). Data are expressed as fold increase and reported as mean ± standard deviation (SD) of three independent experiments.

3.3.5 AChE and BuChE inhibition in vitro

Enzyme activity of EeAChE (E.C. 3.1.1.7, type V-S, purified from *Electrophorus electricus*) and eqBuChE (E.C. 3.1.1.8, purified from equine serum) was assayed kinetically by Ellman's method [30] in 96-well plates, as previously described [25,31], with minor modifications. Compound samples were dissolved at 0.05 M in DMSO and diluted in sodium phosphate buffer (SPB, 0.1 M, pH 7.4) immediately before use (final DMSO less than 0.2% v.v.). All other assay reagents were dissolved in SPB. The final assay volume was 200 µL; three wells were used per condition in each experiment. Sequential additions were: 20 µL of enzyme (0.5 U/mL), 5 µL of 5,5'-dithiobis-(2-nitrobenzoic) acid (10 mM), 100 µL of compound solution (twice the final concentration) and 55 µL of SPB. After ten minutes of incubation, 20 µL of the substrate (acetylthiocholine or butyrylthiocholine iodide, 0.5 M final, or 0.02-0.5 M for the competition experiments) were added, and absorbance was read in a SpectraMax 250 spectrophotometer (Molecular Devices) at 412 nm every 12 s, for 5 min at rt. Progression curves were acquired through SOFTmax PRO 5.0 (Molecular Devices), from which maximum hydrolysis velocity was estimated and analysis performed with Prism (Graphpad). Two six-point inhibition curves were obtained independently for each compound for estimation of average IC_{50}. The substrate competition data from 2-3 experiments were pooled and analyzed by global nonlinear fitting of standard kinetic models [31]. Because all compounds clearly reduced EeAChE V_{max}, only simple (pure) non-competitive and linear mixed inhibition models were fitted, being then compared and selected by likelihood criteria (corrected Akaike information criterion). All reagents were purchased from Sigma-Aldrich (Brazil).

3.3.6 Determination of neuroprotective activity against t-BOOH

The neuroprotective activity was determined by using the MTT assay as previously described [34]. SH-SY5Y cells were seeded in a 96-well plate at 3 x 10^4 cell/well, incubated for 24 h and then treated for 4 h with compound **5k** (2.5 – 10 µM) and *t*-BOOH (50 µM). At the end of incubation, the MTT solution (5 mg/mL) in Hank's balanced salt solution (HBSS) was added for 2 h at 37 °C in 5% CO_2. After washing with HBSS, the formazan crystals were dissolved in 150 µL of isopropanol. The amount of formazan was measured (570 nm, filter reference 690 nm) using a microplate reader (VICTOR™ X3). Data are expressed as absorbance and reported as mean ± SD of three independent experiments.

3.3.7 Determination of neuroprotective activity against OAβ_{1-42}

Aβ_{1-42} peptide (AnaSpec, Fremont, CA, USA) was first dissolved in 1,1,1,3,3,3-hexafluoroisopropanol to 1 mg/mL, sonicated, incubated at room temperature for 24 h, and lyophilized to obtain an unaggregated Aβ_{1-42} peptide film that was solubilized with DMSO and stored at −20°C until use. The aggregation of Aβ_{1-42} peptide into oligomers was performed as previously described [35]. SH-SY5Y cells were seeded in a 96-well plate at 3 × 10^4 cells/well, incubated for 24 h and then treated for 4 h with compound **5k** (5 – 10 µM) and OAβ_{1-42}. At the end of incubation, the neuroprotective

activity, in terms of increase in intracellular MTT granules, was measured by MTT formazan exocytosis assay, as previously described [36]. Data are expressed as absorbance and reported as mean ± SD of three independent experiments.

To evaluate the action of the compounds in the aggregation of $A\beta_{1-42}$ peptide, an in vitro assay was performed using the marker Thioflavin T (ThT) for the aggregates. ThT is a benzothiazole obtained through the methylation of dehydrothiotoluidine with methanol in the presence of hydrochloric acid. It is a dark yellow pigment widely used to visualize and quantify the presence of misfolded protein aggregates (amyloid plaques) both in vivo and in vitro. When linked to structures rich in β-sheets, thioflavin presents an increase in its fluorescence and a characteristic redshift in its emission spectrum, in the 490 nm range when associated with aggregates. The fluorescent behaviour of ThT can be caused by several factors that are capable of influencing the charge distribution of the compound for its excited state, among which are the association with a rigid and highly ordered amyloid structure or a specific chemical interaction with another protein. This marker was diluted in a glycine-NaOH pH 8.5 solution for immediate reading.

The protocol was adapted from Benseny Cases et al (2012) [37]. Firstly, $A\beta_{1-42}$ peptide (Biointech, Brazil) was first dissolved in Milli-Q at pH 10, aliquoted at a concentration of 75 μM, the solution was adjusted to the pH 4-5 with HCl solution (2μL), and stored at -80° C until use. To correctly conduct the test, it is necessary to incubate βA_{1-42} solution for 24 hours at 37 ° C in a dry bath for the amyloid plaques to be formed and then use the peptides to break them. On the day of reading, an opaque 96-well plate was used with 50 μL of the βA-42 solution (75μM), along with 50 μL of ThT, 50 μL of the chosen compounds, and addition of water to complete the wells up to 300 μL. The compounds were tested in 75 μM. In the FlexStation (Molecular Devices, USA), a single point reading, aggregate analyses, was performed with excitation of 450 nm and emission of 490 nm at 37 ° C, followed by a 1-hour kinetic reading, with readings every 15 minutes to observe the interactions every 15 minutes for 1 hour, under the same previous conditions. The whole process was conducted in a dark environment so as not to interfere with ThT fluorescence.

All experiments were carried out in experimental triplicates and three independent experiments. The results were analyzed with the aid of the GraphPad Prism®8.0 software (San Diego, USA). The results obtained when reading the FlexStation were subjected to the ANOVA test (Analysis of Variance), followed by the Bonferroni and Tukey test. For all data, values with $p < 0.05$ were considered significant.

4. Conclusion

A novel series of thirteen *N*-benzyl-(4-hydroxymethyl)piperidine-acyl-hydrazone derivatives was reported as a second generation of hybrid compounds, based on the structural features of donepezil and bioactive alkaloids and synthetic acyl and arylhydrazones, designed as improved multi-target AChE inhibitors. Among all tested compounds, compounds PQM-171 (**5b**), PQM-174 (**5e**), PQM-176 (**5g**) and PQM-181 (**5k**) showed the best *in vitro* selective inhibitory activity of AChE with potencies ranging from 3.3 to 12.0 μM, which were corroborated by i*n silico* docking results. Additional studies

highlighted the highest antioxidant activity for the compound PQM-181 (**5k**), besides its good and selective AChE inhibitory activity. The antioxidant effects of **5k** were also confirmed in human neuronal SH-SY5Y cells against the OS elicited by *t*-BOOH. Interestingly, in the same neuronal cells, compound **5k** showed significant neuroprotective effects against neurotoxicity induced by both soluble $A\beta_{1-42}$ aggregates and *t*-BOOH, evidencing its multifunctional pharmacological profile. Regarding cytotoxicity and predicted ADMET parameters, compound **5k** also showed adequate data related to druggability, suggesting its suitability for drug development against AD.

Acknowledgements

This work was supported by grants from INCT-INOFAR Program (CNPq, Brazil, #465.249/2014-0), FAPEMIG (Brazil, #CEX-APQ-00518-17, #CEX-PPM-00241-15), CNPq (Brazil, #454088/2014-0, #400271/2014-1, #310082/2016-1, #406739/2018-8, #303804/2020-3). This study was also financed in part by the Coordenação de Aperfeiçoamento de Pessoal de Nível Superior - Brazil (CAPES) - Finance Code 001. The authors are also grateful for the fellowships granted by CNPq, FAPEMIG, PIBIC-UFRJ, PIBIC-UNIFAL, PIBICT-UNIFAL.

References

1. Viegas FPD, Simões MCR, Da Rocha MD, Castelli MR, Moreira MS, Junior C V. Doença de alzheimer: Caracterização, evolução e implicações do processo neuroinflamatório. *Rev Virtual Quim*. 2011;3(4):286-306.

2. Alzheimer's Association. Dentro do cérebro: Uma viagem interativa. https://www.alz.org/brain_portuguese/overview.asp. Published 2018.

3. Hardy J, Selkoe DJ. The Amyloid Hypothesis of Alzheimer's Disease: Progress and Problems on the Road to Therapeutics. *Science (80-)*. 2002;297(July):353-357. doi:10.1126/science.1072994

4. Viegas FPD, Simões MCR, Rocha MD da, Castelli MR, Moreira MS, V. Junior C. Alzheimer's Disease: Characterization, Evolution and Implications of the Neuroinflammatory Process. *Rev Virtual Química*. 2011;3(4):286-306. doi:10.5935/1984-6835.20110034

5. Tarozzi A, Morroni F, Merlicco A, et al. Neuroprotective effects of cyanidin 3-O-glucopyranoside on amyloid beta (25-35) oligomer-induced toxicity. *Neurosci Lett*. 2010;473(2):72-76. doi:10.1016/j.neulet.2010.02.006

6. Haass C, Selkoe DJ. Soluble protein oligomers in neurodegeneration: lessons from the Alzheimer's amyloid beta-peptide. *Nat Rev Mol Cell Biol*. 2007;8(2):101-112. doi:10.1038/nrm2101

7. Mattson MP, Magnus T. Ageing and neuronal vulnerability. *Nat Rev Neurosci*. 2006;7(4):278-294. doi:10.1038/nrn1886

8. Scatena R, Martorana GE, Bottoni P, Botta G, Pastore P, Giardina B. An update on pharmacological approaches to neurodegenerative diseases. *Expert Opin Investig Drugs*. 2007;16(1):59-72. doi:10.1517/13543784.16.1.59

9. Šimić G, Babić Leko M, Wray S, et al. Tau protein hyperphosphorylation and aggregation in alzheimer's disease and other tauopathies, and possible neuroprotective strategies. *Biomolecules*. 2016;6(1). doi:10.3390/biom6010006

10. Liu Z, Zhou T, Ziegler AC, Dimitrion P, Zuo L. Oxidative Stress in Neurodegenerative Diseases: From Molecular Mechanisms to Clinical Applications. *Oxid Med Cell Longev*. 2017;2017:1-11. doi:10.1155/2017/2525967

11. Tarozzi A, Merlicco A, Morroni F, et al. Guanosine protects human neuroblastoma cells from oxidative stress and toxicity induced by Amyloid-beta peptide oligomers. *J Biol Regul Homeost Agents*. 2010;24(3):297-306. doi:7 [pii]

12. Zhan Q, Shi X, Wang T, et al. Design and synthesis of thymine modified phthalocyanine for Aβ protofibrils photodegradation and Aβ peptide aggregation inhibition. *Talanta*. 2019;191:27-38. doi:10.1016/j.talanta.2018.08.037

13. Sanabria-Castro A, Alvarado-Echeverría I, Monge-Bonilla C. Molecular Pathogenesis of Alzheimer's Disease: An Update. *Ann Neurosci*. 2017;24(1):46-54. doi:10.1159/000464422

14. Nesi, Giulia; Sestito, Simona; Digiacomo, Maria; Rapposelli S. Oxidative Stress, Mitochondrial Abnormalities and Proteins Deposition: Multitarget Approaches in Alzheimer's Disease. *Curr Top Med Chem*. 2017;17(27):3062-3079. doi:https://doi.org/10.2174/1568026617666170607114232

15. Cavalli A, Bolognesi ML, Minarini A, et al. Multi-target-Directed Ligands To Combat Neurodegenerative Diseases. *J Med Chem*. 2008;51(3):347-372. doi:10.1021/jm7009364

16. Dias KST, Viegas C. Multi-Target Directed Drugs : A Modern Approach for Design of New Drugs for the treatment of Alzheimer ' s Disease. *Curr Neuropharmacol*. 2014;12(3):239-255.

17. Albertini C, Salerno A, de Sena Murteira Pinheiro P, Bolognesi ML. From combinations to multitarget-directed ligands: A continuum in Alzheimer's disease polypharmacology. *Med Res Rev*. 2020. doi:10.1002/MED.21699

18. Prati F, Cavalli A, Bolognesi ML. Navigating the Chemical Space of Multitarget-Directed Ligands: From

Hybrids to Fragments in Alzheimer's Disease. *Molecules*. 2016;21(4):466. doi:10.3390/molecules21040466

19. Bolognesi ML, Rosini M, Andrisano V, et al. MTDL design strategy in the context of Alzheimer's disease: from lipocrine to memoquin and beyond. *Curr Pharm Des*. 2009. doi:10.2174/138161209787315585

20. Gontijo VS, Viegas FPD, Ortiz CJC, et al. Molecular Hybridization as a Tool in the Design of Multi-target Directed Drug Candidates for Neurodegenerative Diseases. *Curr Neuropharmacol*. 2019;18(5):348-407. doi:10.2174/1385272823666191021124443

21. Chen X, Decker M. Multi-target compounds acting in the central nervous system designed from natural products. *Curr Med Chem*. 2013;20(13):1673-1685. doi:10.2174/0929867311320130007

22. Morphy R, Kay C, Rankovic Z. From magic bullets to designed multiple ligands. *Drug Discov Today*. 2004;9(15):641-651. doi:10.1016/S1359-6446(04)03163-0

23. Morphy R, Rankovic Z. Designed Multiple Ligands. An Emerging Drug Discovery Paradigm. *J Med Chem*. 2005;48(21):6523-6543. doi:10.1021/jm058225d

24. Dias Viegas FP, de Freitas Silva M, Divino da Rocha M, et al. Design, synthesis and pharmacological evaluation of N -benzyl-piperidinyl-aryl-acylhydrazone derivatives as donepezil hybrids: Discovery of novel multi-target anti-alzheimer prototype drug candidates. *Eur J Med Chem*. 2018;147:48-65. doi:10.1016/j.ejmech.2018.01.066

25. Lemes LFN, de Andrade Ramos G, de Oliveira AS, et al. Cardanol-derived AChE inhibitors: Towards the development of dual binding derivatives for Alzheimer's disease. *Eur J Med Chem*. 2016;108:687-700. doi:10.1016/j.ejmech.2015.12.024

26. Bano S, Parihar MS. Reduction of lipid peroxidation in different brain regions by a combination of α-tocopherol and ascorbic acid. *J Neural Transm*. 1997;104(11-12):1277-1286. doi:10.1007/BF01294728

27. Cheung J, Rudolph MJ, Burshteyn F, et al. Structures of human acetylcholinesterase in complex with pharmacologically important ligands. *J Med Chem*. 2012;55(22):10282-10286. doi:10.1021/jm300871x

28. Inoue A, Kawai T, Wakita M, Iimura Y, Sugimoto H, Kawakami Y. The simulated binding of (??)-2,3-dihydro-5,6-dimethoxy-2-[[1- (phenylmethyl)-4-piperidinyl]methyl]-1H-inden-1-one hydrochloride (E2020) and related inhibitors to free and acylated acetylcholinesterases and corresponding structure-activity analyses. *J Med Chem*. 1996;39(22):4460-4470. doi:10.1021/jm950596e

29. Friesner RA, Murphy RB, Repasky MP, et al. Extra precision glide: Docking and scoring incorporating a model of hydrophobic enclosure for protein-ligand complexes. *J Med Chem*. 2006;49(21):6177-6196. doi:10.1021/jm051256o

30. Ellman GL, Courtney KD, Andres Jr. V, Featherstone RM. A new and rapid colorimetric determination of acetylcholinesterase activity. *Biochem Pharmacol*. 1961;7:88-95.

31. Castro NG, Costa RS, Pimentel LSB, et al. CNS-selective noncompetitive cholinesterase inhibitors derived from the natural piperidine alkaloid (-)-spectaline. *Eur J Pharmacol*. 2008;580(3):339-349. doi:10.1016/j.ejphar.2007.11.035

32. Montanari S, Mahmoud AM, Pruccoli L, et al. Discovery of novel benzofuran-based compounds with neuroprotective and immunomodulatory properties for Alzheimer's disease treatment. *Eur J Med Chem*. 2019;178:243-258. doi:10.1016/j.ejmech.2019.05.080

33. Pruccoli L, Morroni F, Sita G, Hrelia P, Tarozzi A. Esculetin as a bifunctional antioxidant prevents and counteracts the oxidative stress and neuronal death induced by amyloid protein in sh-sy5y cells. *Antioxidants*. 2020;9(6):1-16. doi:10.3390/antiox9060551

34. Ortiz CJC, Damasio CM, Pruccoli L, et al. Cinnamoyl-N-Acylhydrazone-Donepezil Hybrids: Synthesis and Evaluation of Novel Multifunctional Ligands Against Neurodegenerative Diseases. *Neurochem Res*. 2020;45(12):3003-3020. doi:10.1007/s11064-020-03148-2

35. Tarozzi A, Bartolini M, Piazzi L, et al. From the dual function lead AP2238 to AP2469, a multi-target-directed ligand for the treatment of Alzheimer's disease. *Pharmacol Res Perspect*. 2014;2(2):1-14. doi:10.1002/prp2.23

36. de Freitas Silva M, Tardelli Lima E, Pruccoli L, et al. Design, Synthesis and Biological Evaluation of Novel Triazole N-acylhydrazone Hybrids for Alzheimer's Disease. *Molecules*. 2020;25(14):1-18. doi:10.3390/molecules25143165

37. Benseny-Cases N, Klementieva O, Maly J, Cladera J. Granular Non-Fibrillar Aggregates and Toxicity in Alzheimer's Disease. *Curr Alzheimer Res*. 2012;9(8):962-971. doi:10.2174/156720512803251129